The extracellular matrix regulates granuloma necrosis in tuberculosis

Basim Al shammari[1] , Takayuki Shiomi[2], Liku Tezera[3], Magdalena K Bielecka[3], Victoria Workman[4], Tarangini Sathyamoorthy[1], Francesco Mauri[5], Suwan N Jayasinghe[4], Brian D Robertson[6], Jeanine D'Armiento[2, #] Jon S Friedland[1, #], and Paul T Elkington[1, 3,7*]

[1]Infectious Diseases and Immunity, Department of Medicine, Imperial College London, UK. [2]Department of Medicine, Columbia University, New York, USA. [3]NIHR Respiratory Biomedical Research Unit, Clinical and Experimental Sciences Academic Unit, Faculty of Medicine, University of Southampton, UK. [4]BioPhysics Group, UCL Institute of Biomedical Engineering, UCL Centre for Stem Cells and Regenerative Medicine and UCL Department of Mechanical Engineering, University College London, UK. [5]Histopathology, Department of Medicine, Imperial College London, UK. [6]MRC Centre for Molecular Bacteriology and Infection, Department of Medicine, Imperial College London, UK. [7]Institute for Life Sciences, University of Southampton, UK.

[#]These authors contributed equally

*** Address for correspondence:**

Dr Paul T Elkington
Clinical and Experimental Sciences
University of Southampton, Southampton SO16 1YD
Tel 00 44 23 8079 6671
E-mail: p.elkington@soton.ac.uk

Running title: Tuberculosis and the matrix

Abstract

A central tenet of tuberculosis (TB) pathogenesis is that caseous necrosis leads to extracellular matrix destruction and bacterial transmission. We reconsider the underlying mechanism of TB pathology and demonstrate that collagen destruction may be a critical initial event, causing caseous necrosis as opposed to resulting from it. In human TB granulomas, regions of extracellular matrix destruction map to areas of caseous necrosis. In mice, transgenic expression of human matrix metalloproteinase-1 causes caseous necrosis, the pathological hallmark of human TB. Collagen destruction is the principal pathological difference to wild type mice, whereas the release of pro-inflammatory cytokines does not differ, demonstrating that collagen breakdown may lead to cell death and caseation. To investigate this hypothesis, we developed a 3-dimensional cell culture model of TB granuloma formation utilising bioelectrospray technology. Collagen improved survival of *Mycobacterium tuberculosis*-infected cells analyzed by LDH release, propidium iodide staining and total viable cells. Taken together, these findings suggest that collagen destruction is an initial event in TB immunopathology, leading to caseous necrosis and compromising the immune response, revealing a previously unappreciated role for the extracellular matrix in regulating the host-pathogen interaction.

Abstract word count: 184

Keywords: Tuberculosis, extracellular matrix, matrix metalloprotease, immunopathology

Introduction

The intensive biomedical research effort to develop new vaccination approaches and shorter treatment regimens for tuberculosis (TB) have not yet resulted in significant changes to disease management [1-3], suggesting that paradigms of pathogenesis may be incomplete. The pathophysiological hallmark of TB is caseous necrosis, which is thought to result from *Mycobacterium tuberculosis* (Mtb)-mediated macrophage cell death [4-6]. An excessive pro-inflammatory immune response may exacerbate tissue destruction [7], and this concept of pathology informs novel vaccine and immunomodulatory strategies [8, 9].

In this model of TB pathology, caseous necrosis is proposed to cause tissue destruction, leading to lung cavitation and transmission of infection [10, 11]. This long-established paradigm primarily derives from classical experiments in the rabbit model of *Mycobacterium bovis* infection, where large tubercules develop and then rupture into the airways [12]. However, dissection of the precise sequence of events is limited by suitable animal models, since caseous necrosis is generally not observed in immunocompetent mice [13]. Caseous necrosis is observed in TB granulomas of humanised mice engrafted with fetal human liver and thymus tissue [14], while large regions of necrosis may develop in mice that control Mtb proliferation poorly and develop a very high mycobacterial load [15]. However, in human granulomas mycobacteria are very infrequent [16], and therefore in human disease pathology is initially driven by a low mycobacterial load.

We have previously demonstrated that MMP-1 expressing mice develop collagen destruction within granulomas when infected with the standard laboratory strain, Mtb H37Rv, and this collagen destruction occurred in the absence of caseous necrosis [17]. However, the relationship between matrix destruction and the cell death that forms caseous necrosis have not been systematically examined, nor the consequences of matrix destruction on the interaction between host immune cells and Mtb. We reconsider the sequence of events driving immunopathology in TB by studying human

lung biopsy tissue, mice expressing human MMPs and 3-dimensional cell culture systems, and conclude that collagen destruction is an early event that increases host cell death.

Methods

Ethics statement: The project was approved by the Hammersmith and Queen Charlotte's & Chelsea Research Ethics Committee, London (ref 07/H0707/120). Lung biopsy tissue was taken as part of routine clinical care and processed for standard diagnostic testing. The residual tissue blocks not required for diagnostic purposes were analyzed in this study and were released from the Hammersmith Hospitals NHS Trust Human Biomaterials Resource centre. The ethics committee approved the analysis of this tissue without individual informed consent since it was surplus archived tissue taken as part of routine care. All animal experiments were approved by the Home Office of the United Kingdom, which is responsible for approving laboratory animal care and experiments in the UK, under project licence PPL 70-7160. All experiments were performed in accordance with the UK Animal (Scientific Procedures) Act 1986 in the containment level 3 animal facility at Imperial College London. For analysis of blood from healthy donors, this work was approved by the National Research Ethics Service committee South Central - Southampton A (ref 13 SC 0043) and all donors gave written informed consent.

Extracellular matrix staining in human lung biopsies: Lung biopsies from patients under investigation for probable lung cancer who had pulmonary TB diagnosed as a result of the biopsy appearances were studied. All patients had caseous necrosis, the pathognomonic appearance of tuberculosis, and responded well to standard antibiotic treatment. Staining for Masson's Trichrome, Picrosirius red and Elastin Van Gieson was performed according to standard protocols.

Mouse *M. tuberculosis* infection protocol: All mice were bred on the C57BL6 background, which is relatively resistant to infection with Mtb. Mice expressing human MMP-1 and -9 under control of the scavenger receptor A promoter-enhancer and wild-type littermates were infected intranasally with 5,000 colony forming units *M. tuberculosis* that had recently been isolated from a patient with pulmonary TB [18]. Preliminary studies demonstrated that this protocol reliably produced a pulmonary deposition of approximately 500 CFU and caused giant cell formation, a characteristic

feature of human disease not caused by Mtb H37Rv in C57BL6 mice. In each experiment, there were a minimum 5 mice per group and 3 separate experiments were performed. Mice were checked regularly for signs of distress and weighed fortnightly. Mice were sacrificed by terminal overdose of anaesthetic at 22 weeks and dissected as previously described [17]. For protein analysis and colony counting, one lobe was homogenised in 1ml PBS. Colony counting was performed by plating on Middlebrook 7H11 agar (BD Biosciences). Lung homogenate and BALF was sterilized through a 0.2μm filter (Millipore) [19].

Luminex analysis: MMP and cytokine concentrations were analyzed on a Bioplex 200 platform (Bio-Rad, Hemel Hempstead, U.K.) according to manufacturer's protocol. MMP concentrations were analysed by the MMP Fluorokine multianalyte profiling (R&D Systems, Abingdon, UK) and cytokine concentrations were measured using the Cytokine mouse panel (Invitrogen, UK).

2-Dimensional *In Vitro* Granuloma (IVG) model: The model described by Altare's group was adapted [20]. Peripheral Blood Mononuclear Cells (PBMCs) were isolated from single donor buffy coats from the National Blood Transfusion Service (Colindale, UK) or from healthy volunteers. Leukocytes were isolated by density centrifugation over Ficoll Paque (Amersham Biosciences, UK). Total PBMCs were plated in 24 well plate at $1x10^6$ cells/well in 10% AB serum in RPMI supplemented with 2mM glutamine and 10μg/ml ampicillin. PBMCs were infected with Mtb at a multiplicity of infection (MOI) of 0.001.

DQ collagen degradation assay: PBMCs were resuspended in collagen mix solution: 8 parts sterile collagen type I (Advanced BioMatrix, San Diego, CA) with DQ collagen (Invitrogen, Paisley, UK) in 1:7 ratio, and 1 part of sterile 10X RPMI, NaOH in HEPES and AB serum. pH was corrected to 7.0 using 7.5% NaHCO3. $1x10^6$ PBMCs were seeded in 4-well cover glass bottom chamber slides (PAA laboratories) and *M.tb* was added at MOI of 0.001 to infection wells. Slides were incubated and observed under confocal microscope (Leica.

Green Fluorescent collagen degradation assay: 4-well glass bottom chamber slides (PAA laboratories) were coated with 0.005% poly-L-lysine (Sigma, Poole, UK), washed sequentially with

PBS, 0.5% glutaraldehyde (BDH) then PBS. Wells were coated with collagen-FITC solution (Sigma, 1mg/ml) in 0.1M acetic acid solution, washed with PBS then sodium borohydride solution (Sigma) and sterile HBSS. Wells were seeded with PBMCs, infected with *M.tb* and observed under confocal microscope (Leica Microsystems).

Lactate dehydrogenase (LDH) assay: Cell culture supernatants were harvested, sterile filtered (Millipore, UK) and analyzed as per manufacturers' instructions (Roche, Burgess Hill, UK).

Agar 3-dimensional cell culture model: Soft agar (1.5%, Sigma) was heated in a microwave for 2 minutes and warmed to 50ºC. A final agar concentration of 0.7% was prepared with 10x RPMI 1640, AB serum (10%), 1M HEPES, 7.5% $NaHCO_3$ and distilled water. PBMCs were incorporated within the agar +/- collagen and the gel was allowed to set at 37ºC. RPMI with 10% AB serum was added to the wells and sampled at predetermined time points.

Cell Encapsulation using Electrostatic Bead Generator: PBMCs were isolated and embedded into alginate microspheres using an electrostatic bead generator as described [21] (Nisco, Zurich, Switzerland). Briefly, PBMC were mixed with sterile alginate mix (3%, Sigma, UK or Pronova UP MVG alginate , NovaMatrix, Norway) in HBSS without Ca/Mg, 1M HEPES and 7.5% $NaHCO_3$ to a final concentration of $5x10^6$ cells/ml. Purified human collagen solution (VitroCol, Advanced BioMatrix) was added at 1mg/ml for alginate-collagen microspheres. Mtb-stimulated microspheres were generated by adding either UV killed *Mycobacterium tuberculosis* H37Rv or bioluminescent Mtb H37Rv expressing the Lux operon, at multiplicity of infection (MOI) 0.1, to the alginate solution prior to microsphere generation.

Alginate suspension containing cells +/- Mtb +/- collagen was injected via a Harvard syringe driver into the bead generator at 10ml/hr, with a 0.7mm external diameter bioelectrospray needle. Microspheres were formed by ionotropic gelling in 100mM calcium chloride. Microspheres were then washed twice with HBSS and then placed in RPMI supplemented with 10% AB serum at 37ºC. Supernatant surrounding the microspheres was harvested at defined time points.

Immunofluorescence and Confocal Imaging: Microspheres were fixed in 4% paraformaldehyde, washed in PBS and then stained with DAPI (4',6-diamidino-2-phenylindole) or calcein. Confocal images were acquired on a Leica SPE microscope with an APO 40 X 1.15 NA oil immersion lens.

Flow cytometry: Cells were extracted from microspheres by dissolving in 15mM EDTA in PBS for 10 minute at 37^{o}C. Cells were suspended in PBS containing 50µg/ml propidium idodide (PI), and the fluorescence was analyzed by flow cytometry (BD Accuri™ C6 flow cytometer). Three replicates were taken for each experiment and 10,000 cells were acquired for each sample. Experiments were repeated at least three times.

Cell viability assay: Microspheres containing PBMCs infected with UV-killed Mtb at MOI of 0.1 were generated from alginate, alginate-collagen (Advanced BioMatrix) or alginate-gelatin (Sigma). Microspheres were incubated in 96-well plates for 4 days at 37^{o}C. Cell viability was analyzed using the CellTiter-Glo® 3D Cell Viability Assay (Promega) according to manufacturer's instructions. Luminescence was analyzed by Glomax Discover (Promega).

Statistics: Paired groups were compared by Students t-test, while multiple groups were analyzed by one-way ANOVA. Differences were considered significant at $P < 0.05$.

Results

Caseous necrosis maps to regions of collagen destruction in human pulmonary granulomas

First, we investigated extracellular matrix integrity and caseous necrosis in lung granulomas from patients with pulmonary TB (Figure 1 and Supplemental figure 1). Sirius red staining demonstrated that collagen was intact where cells had normal morphology, whereas in areas of caseous necrosis no collagen was visualised (Figure 1A and B). Elastin van Giesen staining demonstrated no elastin was present in these regions (Figure 1C and D). Similarly, Masson's Trichrome staining showed that extracellular matrix was absent in areas of caseous necrosis (Supplemental Figure 1). Therefore, in patients with pulmonary TB, caseous necrosis and extracellular matrix destruction are observed concurrently, but whether cell death or matrix destruction is the initial pathological event cannot be determined.

Expression of human MMP-1 in the mouse causes caseous necrosis in TB granulomas

To address the relationship between matrix destruction and cell death, we infected mice expressing human matrix metalloproteinase (MMP)-1 under control of the scavenger receptor A promoter enhancer [22] with a clinical strain of Mtb recently isolated from a patient with pulmonary TB. All mice were bred on the C57BL6 background, which is relatively resistant to mycobacterial infection, and were infected with 5,000 CFU intranasally, resulting in a pulmonary infectious dose of 500 CFU. In preliminary studies, we demonstrated that this strain caused typical pathological features of human TB not observed after infection with the standard laboratory Mtb H37Rv in C57BL6 mice. C57BL6 mice expressing human MMP-9 regulated by the same promoter acted as controls for the transgenic expression of a human MMP. In all infected mice, multinucleate giant cells were observed within granulomas, implying that multinucleate giant cells result from infection with Mtb that has not undergone prolonged laboratory subculture (Figure 2A-C). No difference in colony counts or weight loss occurred between strains, demonstrating that human MMP expression did not modulate control of

Mtb growth (Figure 2D-E). Total lung inflammation was similar between mice (Supplemental figure 2) and Mtb was visualised on Ziehl-Neelsen staining of granulomas in each mouse strain (Supplemental figure 3). Mtb infection up-regulated human MMP-1 and MMP-9 expression in the respective transgenic mice (Figure 2F-G). In the MMP-1 expressing mice, areas of tissue destruction were observed within the centre of granulomas (Figure 2K-M), that did not occur in wild type or MMP-9 mice (Figure 2H-J and N-P). These regions contained amorphous debris with no cellular structure, typical of caseous necrosis observed in human TB. Therefore MMP-1-expressing mice demonstrate pathology characteristic of human TB which is not seen in other immunocompetent mice of diverse genetic background [13] unless either humanised or in the context of very high mycobacterial load [14, 15].

To determine whether caseous necrosis resulted from an imbalance in TH1/TH2 immunity as has been postulated [6], we profiled cytokines and chemokines in lung homogenate and bronchial lavage fluid by luminex array. Mtb infection up-regulated TNF-α, IL-1β, IL-12, IFN-γ, MCP-1 and IP-10 in all mouse strains, but no difference in cytokine profile was demonstrated (Figure 3A-F). This suggested that the observed caseous necrosis did not result from MMP-1 expression having an immunomodulatory effect. IL-6 concentrations were below the level of sensitivity of the assay even at maximal sensitivity. The only difference between the MMP-1 mice and their wild-type littermates is the expression of a collagenase, leading us to examine extracellular matrix integrity within granulomas. In all areas of caseous necrosis, collagen was destroyed (Figure 3H), whereas in wild type mice and MMP-9 mice the extracellular matrix was intact and cells appeared viable within TB granulomas (Figure 3G and I, high magnification images Supplemental figure 4).

Collagen improves survival of Mtb-infected human cells

The development of caseous necrosis in MMP-1 mice suggested that the initial event in TB immunopathology is collagen destruction, which then leads to cell death, as opposed to the current

paradigm that collagen destruction occurs secondary to cell death. To test this hypothesis, we first analyzed a 2-dimensional cell-culture *in vitro* granuloma model incorporating PBMCs and live Mtb [23]. Human granulomas contain very few mycobacteria relative to inflammatory cells [16], and so a low MOI was utilised to reflect clinical disease. Granulomas formed over time (Figure 4A). Mtb infection increased MMP and cytokine expression (Figure 4B-C and Supplemental figure 5). To quantitate the functional effect of MMP activity on matrix turnover, cells were plated on slides coated with DQ-labelled collagen, which becomes fluorescent when degraded, or fluorescent collagen, which loses fluorescence when cleaved. The increased MMP activity caused collagen degradation by both assays (Figure 4D-E). Addition of human collagen to the cell culture media improved cellular survival after Mtb infection (Figure 4F). However, cell-matrix interactions occur in a 3-dimensional framework and therefore we studied 3-D granuloma models impregnated with diverse matrices. In an agar 3-D model, incorporation of collagen improved cellular survival after Mtb stimulation compared to cells in an agar matrix without collagen (Figure 4G).

To further investigate this observation, we developed a 3-dimensional cell culture model of TB granuloma formation, since cell-matrix interactions occur in 3 dimensions. This model permitted investigation of the hypothesis that matrix composition regulates the host-pathogen interaction without the need for extensive animal modelling. We utilised a bioelectrospray system to generate microspheres incorporating alginate, which cross-links in a gelling bath containing calcium chloride, and this system permits regulation of the cellular and matrix fibrillar composition within the microspheres (Figure 5A-B) [21]. Monocytes within the microspheres phagocytosed Mtb (Figure 5C) and progressive cellular aggregation occurred in infected microspheres over time (Figure 5D). Mtb infection led to a progressive increase in chemokine and MMP accumulation in the cell culture medium, demonstrating that inflammatory mediators increased in human TB are induced within this model (Figure 5E-F). To determine whether the matrix regulated cellular survival, human type I collagen was incorporated into microspheres. Cells in collagen-impregnated microspheres survived better when infected with Mtb, analyzed by LDH release (Figure 5G-H) and flow cytometry (Figure

5I). Furthermore, total viable cell numbers in collagen containing microspheres were higher than in alginate-only microspheres (Figure 5J). In contrast, incorporation of gelatin into the microspheres did not increase cellular viability (Figure 5J). These data confirm that cells adherent to collagen fibrils have greater survival when infected with Mtb than those without extracellular matrix contact.

Discussion

Taken together, our human, mouse and cellular data implicate that collagen destruction is an early event in TB pathogenesis, leading to the development of caseous necrosis and skewing the immune response in favour of the pathogen. Collagen breakdown reduces the survival of Mtb-infected cells. Collagen had a more pronounced effect on cell survival in 3-D cell culture than 2-D cell culture, consistent with the emerging concept that analysis of cell biology in three dimensions may recapitulate *in vivo* cellular behaviour more accurately than in standard tissue culture [24]. Collagen destruction preceding caseation in TB is opposite to the widely held disease paradigm that extracellular matrix destruction is a consequence of caseous necrosis [4, 6], and leads to a novel concept of TB immunopathology whereby extracellular matrix destruction is the initial pathological event (Figure 6). This model is consistent with studies in cancer, where the extracellular matrix is known to be a cell survival factor [25]. However, human biopsy studies only provide a single disease time point and consequently cannot determine the precise chronology of events. Ultimate proof of this concept will require MMP inhibition studies in an animal model that recapitulates the key pathological features of human TB, such as the rabbit [26], with demonstration that collagenase inhibition reduces Mtb-driven immunopathology.

Matrix regulation of the host immune response to TB has widespread implications, but the role of the matrix in TB tends not to be considered [4, 6, 27]. We demonstrated that collagen increased survival of cells infected with Mtb, whereas gelatin did not, showing that intact collagen fibrils are required. The extracellular matrix has numerous components, such as fibronectin, elastin, laminin, other collagen subtypes, proteoglycans and hyaluronan [28], and similarly these molecules may modulate the host-pathogen interaction in TB [29]. Such cell-matrix interactions can be predicted to affect multiple key processes in the immune response to TB. For example, the extracellular matrix can modulate phagolysosomal fusion [30], pro-inflammatory cytokine secretion [31], autophagy [32] and immune cell activation [29]. Furthermore, cell-matrix interactions regulate cell survival [33], which

is central to the host-pathogen interaction in TB [34]. In epithelial cells, integrin-dependent activation of intracellular signalling pathways via the EGF receptor regulate cellular survival [25, 35] and in monocytes matrix adhesion modulates gene expression profiles via integrins [36]. However, in TB the *in vitro* experiments dissecting intracellular signalling pathways have almost entirely been performed in the absence of extracellular matrix.

Certain transgenic mouse models of TB may develop large regions of tissue destruction in the context of very high mycobacterial loads [15]. Lesions are marked by pronounced neutrophil infiltration, and therefore matrix destruction may be driven by MMP-8 (neutrophil collagenase), since neutrophils are the only cells that contain pre-synthesised MMPs. Therefore, different proteases from diverse cell types may drive pathology at different stages of TB disease. We focused on MMP-1, since unbiased analysis of MMPs in TB suggest that this is a dominant collagenase [26, 37, 38], but at late stages of infection neutrophil-derived MMP-8 is also likely to drive collagen destruction [39]. Similarly, stromal cells such as epithelial cells and fibroblasts may be key sources of MMPs in inflammatory foci [40]. Our data suggest that macrophage-derived MMP-1 causes initial collagen destruction within the granuloma, leading to reduced cell survival. The standard laboratory strain, Mtb H37Rv, did not cause caseous necrosis nor multinucleate giant cell formation in infected mice, whereas these pathologies were observed after infection with a recently isolated clinical strain of TB. This implies that the prolonged laboratory culture of H37Rv since its isolation from a patient in 1905 [41] has resulted in loss of currently unidentified factors that cause giant cell formation and caseous necrosis despite being able to proliferate rapidly.

The process of caseation is likely to involve additional pathological processes that cannot be dissected our *in vitro* model. Diverse animal models demonstrate that TB granulomas are hypoxic [42] and in man, vascular supply to areas of TB infection are occluded [43]. Hypoxia and inflammation have a complex interplay, and hypoxia can augment MMP release [44]. The bioelectrospray model currently

incorporates peripheral blood mononuclear cells, and so cannot investigate the role of neutrophils or stromal cells, which all contribute to TB pathogenesis [39, 45]. More advanced *ex vivo* organ culture, or *in vivo* experiments in an animal model where pathology reflects disease in man, will be required to fully dissect the interplay of matrix destruction, hypoxia and intercellular signalling.

A central role for matrix breakdown in TB pathology is supported by unbiased approaches. For example, a study comparing the macrophage gene expression profile from patients with pulmonary TB to latently infected individuals identified MMP-1 as the most divergently regulated gene [46], suggesting that excessive matrix destruction predisposes to developing TB. Similarly, MMP-1 is one of the most highly up-regulated genes in infected human lung tissue [37]. A recent aptamer-based approach identified protease-anti-protease balance and tissue remodelling as two key pathways that change during TB treatment, whereas cytokine pathways were not highly represented [47]. All TB treatments in the pre-antibiotic era, such as artificial pneumothorax, plombage and thoracoplasty, centred on cavity collapse, and these had a cure rate of up to 70% [48], demonstrating that macroscopic stabilisation of the extracellular matrix can improve host control of Mtb infection.

Tissue damage is emerging as a central determinant of the outcome of the host-pathogen interaction in other lung infections, such as bacterial-viral co-infection [49], supporting the hypothesis that preserving matrix integrity is fundamental to an effective response to infection. Our data demonstrate that destruction of the lung extracellular matrix is likely to be an earlier event in the pathogenesis of TB than previously thought. Host-directed therapies are emerging as a novel paradigm in TB treatment [50]. Matrix stabilisation strategies in TB may not only reduce morbidity and mortality, but may also help restore an efficacious immune response to Mtb infection.

Manuscript word count: 3,500

Acknowledgements: We thank G. Thwaites for providing the Indo-Oceanic strain of Mtb and Siouxsie Wiles and Nuria Andreu for the luminescent Mtb.

Footnotes

Conflict of interest statement: The authors declare no conflict of interest.

Funding: This work was supported by a King Abdullah Scholarship Program (BAS), a HEFCE New Investigator award (PE), the US NIH (AI102239) and the NC3Rs (NC/L001039/1). PE and JSF are grateful for support from the National Institute for Health Research (NIHR) Biomedical Research Centre (BRC) funding scheme at Imperial College.

Some of this work has been presented at the 2014 Keystone "Novel Therapeutic Approaches to Tuberculosis" meeting.

References

1. Tameris MD, Hatherill M, Landry BS, et al. Safety and efficacy of MVA85A, a new tuberculosis vaccine, in infants previously vaccinated with BCG: a randomised, placebo-controlled phase 2b trial. Lancet **2013**; 381:1021-8.

2. Johnson JL, Hadad DJ, Dietze R, et al. Shortening treatment in adults with noncavitary tuberculosis and 2-month culture conversion. Am J Respir Crit Care Med **2009**; 180:558-63.

3. Zumla A, Hafner R, Lienhardt C, Hoelscher M, Nunn A. Advancing the development of tuberculosis therapy. Nat Rev Drug Discov **2012**; 11:171-2.

4. Cooper AM. Cell-mediated immune responses in tuberculosis. Annu Rev Immunol **2009**; 27:393-422.

5. Barry CE, 3rd, Boshoff HI, Dartois V, et al. The spectrum of latent tuberculosis: rethinking the biology and intervention strategies. Nat Rev Microbiol **2009**; 7:845-55.

6. O'Garra A, Redford PS, McNab FW, Bloom CI, Wilkinson RJ, Berry MP. The immune response in tuberculosis. Annu Rev Immunol **2013**; 31:475-527.

7. Cooper AM, Torrado E. Protection versus pathology in tuberculosis: recent insights. Curr Opin Immunol **2012**; 24:431-7.

8. Uhlin M, Andersson J, Zumla A, Maeurer M. Adjunct immunotherapies for tuberculosis. J Infect Dis **2012**; 205 Suppl 2:S325-34.

9. Kaufmann SH. Future vaccination strategies against tuberculosis: thinking outside the box. Immunity **2010**; 33:567-77.

10. Dye C, Williams BG. The population dynamics and control of tuberculosis. Science **2010**; 328:856-61.

11. Russell DG, Barry CE, 3rd, Flynn JL. Tuberculosis: what we don't know can, and does, hurt us. Science **2010**; 328:852-6.

12. Dannenberg AM, Jr., Sugimoto M. Liquefaction of caseous foci in tuberculosis. Am Rev Respir Dis **1976**; 113:257-9.

13. Young D. Animal models of tuberculosis. Eur J Immunol **2009**; 39:2011-4.

14. Calderon VE, Valbuena G, Goez Y, et al. A humanized mouse model of tuberculosis. PLoS ONE **2013**; 8:e63331.

15. Pan H, Yan BS, Rojas M, et al. Ipr1 gene mediates innate immunity to tuberculosis. Nature **2005**; 434:767-72.

16. Park DY, Kim JY, Choi KU, et al. Comparison of polymerase chain reaction with histopathologic features for diagnosis of tuberculosis in formalin-fixed, paraffin-embedded histologic specimens. Arch Pathol Lab Med **2003**; 127:326-30.

17. Elkington P, Shiomi T, Breen R, et al. MMP-1 drives immunopathology in human tuberculosis and transgenic mice. J Clin Invest **2011**; 121:1827-33.

18. Krishnan N, Malaga W, Constant P, et al. Mycobacterium tuberculosis lineage influences innate immune response and virulence and is associated with distinct cell envelope lipid profiles. PLoS ONE **2011**; 6:e23870.

19. Elkington PT, Green JA, Friedland JS. Filter sterilization of highly infectious samples to prevent false negative analysis of matrix metalloproteinase activity. J Immunol Methods **2006**; 309:115-9.

20. Puissegur MP, Botanch C, Duteyrat JL, Delsol G, Caratero C, Altare F. An in vitro dual model of mycobacterial granulomas to investigate the molecular interactions between mycobacteria and human host cells. Cell Microbiol **2004**; 6:423-33.

21. Workman VL, Tezera LB, Elkington PT, Jayasinghe SN. Controlled Generation of Microspheres Incorporating Extracellular Matrix Fibrils for Three-Dimensional Cell Culture. Advanced Functional Materials **2014**; 24:2648-57.

22. Lemaitre V, O'Byrne TK, Borczuk AC, Okada Y, Tall AR, D'Armiento J. ApoE knockout mice expressing human matrix metalloproteinase-1 in macrophages have less advanced atherosclerosis. J Clin Invest **2001**; 107:1227-34.

23. Puissegur MP, Lay G, Gilleron M, et al. Mycobacterial lipomannan induces granuloma macrophage fusion via a TLR2-dependent, ADAM9- and beta1 integrin-mediated pathway. J Immunol **2007**; 178:3161-9.

24. Schwartz MA, Chen CS. Cell biology. Deconstructing dimensionality. Science **2013**; 339:402-4.

409 25. Meredith JE, Jr., Fazeli B, Schwartz MA. The extracellular matrix as a cell survival factor. Mol
410 Biol Cell **1993**; 4:953-61.
411 26. Kubler A, Luna B, Larsson C, et al. Mycobacterium tuberculosis dysregulates MMP/TIMP
412 balance to drive rapid cavitation and unrestrained bacterial proliferation. J Pathol **2015**; 235:431-44.
413 27. Elkington PT, D'Armiento JM, Friedland JS. Tuberculosis immunopathology: the neglected role
414 of extracellular matrix destruction. Sci Transl Med **2011**; 3:71ps6.
415 28. Davidson JM. Biochemistry and turnover of lung interstitium. Eur Respir J **1990**; 3:1048-63.
416 29. Sorokin L. The impact of the extracellular matrix on inflammation. Nat Rev Immunol **2010**;
417 10:712-23.
418 30. Newman SL, Gootee L, Kidd C, Ciraolo GM, Morris R. Activation of human macrophage
419 fungistatic activity against Histoplasma capsulatum upon adherence to type 1 collagen matrices. J
420 Immunol **1997**; 158:1779-86.
421 31. Merline R, Moreth K, Beckmann J, et al. Signaling by the matrix proteoglycan decorin controls
422 inflammation and cancer through PDCD4 and MicroRNA-21. Science signaling **2011**; 4:ra75.
423 32. Lock R, Debnath J. Extracellular matrix regulation of autophagy. Curr Opin Cell Biol **2008**;
424 20:583-8.
425 33. Buchheit CL, Rayavarapu RR, Schafer ZT. The regulation of cancer cell death and metabolism by
426 extracellular matrix attachment. Seminars in cell & developmental biology **2012**; 23:402-11.
427 34. Behar SM, Divangahi M, Remold HG. Evasion of innate immunity by Mycobacterium
428 tuberculosis: is death an exit strategy? Nat Rev Microbiol **2010**; 8:668-74.
429 35. Moro L, Venturino M, Bozzo C, et al. Integrins induce activation of EGF receptor: role in MAP
430 kinase induction and adhesion-dependent cell survival. Embo J **1998**; 17:6622-32.
431 36. de Fougerolles AR, Chi-Rosso G, Bajardi A, Gotwals P, Green CD, Koteliansky VE. Global
432 expression analysis of extracellular matrix-integrin interactions in monocytes. Immunity **2000**;
433 13:749-58.
434 37. Kim MJ, Wainwright HC, Locketz M, et al. Caseation of human tuberculosis granulomas
435 correlates with elevated host lipid metabolism. EMBO Mol Med **2010**; 2:258-74.

436 38. Mehra S, Pahar B, Dutta NK, et al. Transcriptional reprogramming in nonhuman primate (rhesus
437 macaque) tuberculosis granulomas. PLoS ONE **2010**; 5:e12266.
438 39. Eum SY, Kong JH, Hong MS, et al. Neutrophils are the predominant infected phagocytic cells in
439 the airways of patients with active pulmonary TB. Chest **2010**; 137:122-8.
440 40. Elkington PT, Emerson JE, Lopez-Pascua LD, et al. Mycobacterium tuberculosis up-regulates
441 matrix metalloproteinase-1 secretion from human airway epithelial cells via a p38 MAPK switch. J
442 Immunol **2005**; 175:5333-40.
443 41. Bifani P, Moghazeh S, Shopsin B, Driscoll J, Ravikovitch A, Kreiswirth BN. Molecular
444 characterization of Mycobacterium tuberculosis H37Rv/Ra variants: distinguishing the mycobacterial
445 laboratory strain. J Clin Microbiol **2000**; 38:3200-4.
446 42. Via LE, Lin PL, Ray SM, et al. Tuberculous granulomas are hypoxic in guinea pigs, rabbits, and
447 nonhuman primates. Infect Immun **2008**; 76:2333-40.
448 43. Dastur DK, Dave UP. Ultrastructural basis of the vasculopathy in and around brain tuberculomas.
449 Possible significance of altered basement membrane. Am J Pathol **1977**; 89:35-50.
450 44. Lee YA, Choi HM, Lee SH, et al. Hypoxia differentially affects IL-1beta-stimulated MMP-1 and
451 MMP-13 expression of fibroblast-like synoviocytes in an HIF-1alpha-dependent manner.
452 Rheumatology (Oxford) **2012**; 51:443-50.
453 45. Volkman HE, Pozos TC, Zheng J, Davis JM, Rawls JF, Ramakrishnan L. Tuberculous granuloma
454 induction via interaction of a bacterial secreted protein with host epithelium. Science **2010**; 327:466-
455 9.
456 46. Thuong NT, Dunstan SJ, Chau TT, et al. Identification of tuberculosis susceptibility genes with
457 human macrophage gene expression profiles. PLoS Pathog **2008**; 4:e1000229.
458 47. De Groote MA, Nahid P, Jarlsberg L, et al. Elucidating novel serum biomarkers associated with
459 pulmonary tuberculosis treatment. PLoS ONE **2013**; 8:e61002.
460 48. Sellors TH. The results of thoracoplasty in pulmonary tuberculosis. Thorax **1947**; 2:216-23.
461 49. Jamieson AM, Pasman L, Yu S, et al. Role of tissue protection in lethal respiratory viral-bacterial
462 coinfection. Science **2013**; 340:1230-4.

463 50. Mayer-Barber KD, Andrade BB, Oland SD, et al. Host-directed therapy of tuberculosis based on
464 interleukin-1 and type I interferon crosstalk. Nature **2014**; 511:99-103.

465

466

Figure legends

Figure 1: **Lung matrix destruction and caseous necrosis co-localize in human pulmonary granulomas.** Lung biopsies from patients under investigation for lung carcinoma but with a final diagnosis of TB made on histological analysis were stained by Picrosirius red (A, B; collagen fibrils stain red), and Elastin van Gieson (C, D; elastin fibrils stain blue). Arrowheads designate areas of caseous necrosis. Collagen and elastin fibrils are absent in all regions of caseous necrosis. Images are representative of 5 TB patient lung biopsies that were studied. Scale bars 100μm.

Figure 2: Mice expressing human MMP-1 develop regions of caseous necrosis in TB granulomas. Mice expressing human MMP-1, MMP-9 or wild-type littermates were infected with an Indo-Oceanic strain of Mtb recently isolated from a patient with pulmonary TB. Mice were sacrificed 22 weeks after infection. (A-C) All mice strains developed multinucleate giant cells in regions of macrophage infiltration (Arrowheads). (D) No difference in mycobacterial growth was observed between mice strains. Horizontal line demonstrates mean with bars SD. (E) Mouse weights did not differ between strains during the course of infection. Circles denote wild type mice, squares MMP-1 and triangles MMP-9-expressing mice, plotting mean and bars SD. (F, G) Infection up-regulated human MMP-1 and MMP-9 in lung homogenates of the respective transgenic mice. Mean values +/- SEM are shown. (H-P) In the MMP-1 mice, regions of tissue destruction developed (Arrowheads), with amorphous central material typical of human caseous necrosis (K, L, M), which was not observed in similar granulomas in wild type (H, I, J) or MMP-9 mice (N, O, P). The experiment was performed 3 times, with a minimum of 5 mice per group. Scale bars 25μm.

Figure 3: Cytokine secretion does not differ between MMP-1 and wild type mice, but collagen is absent in regions of caseous necrosis. (A-F) Concentrations of TNF-α, IL-1β, IL-12, IFN-γ, MCP-1

and IP-10 were measured in mouse lung homogenates at 22 weeks after infection by Luminex array. Mtb infection up-regulated each of these pro-inflammatory mediators in all infected mice, but there were no significant differences related to the genotype of the mice. Open bars, uninfected mice, filled bars Mtb-infected mice. Mean +/- SEM values are shown. (G-I) Total collagen was analyzed by Picrosirius red staining. In wild type (G) and MMP-9 (I) mice, alveolar wall collagen remained intact in regions of macrophage infiltration. However, in MMP-1 mice, collagen was destroyed and co-localized with regions of caseous necrosis (H). Data are representative of 5 mice per group infected in 3 independent experiments. Scale bars 50μm.

Figure 4: Collagen improves survival of Mtb-infected cells in a 2-dimensional primary human cell culture system. Primary human PBMCs were infected with Mtb H37Rv in 24-well tissue culture plates and observed for 15 days. (A) Cellular aggregates develop in Mtb-infected wells by day 4. (B-C) Mtb infection increases secretion of TNF-α and MMP-1 in cell culture supernatants analyzed by luminex array. (D) Aggregates cause pericellular collagen destruction, analyzed by co-culture with DQ-labelled collagen, which gains fluorescence when cleaved or (E) fluorescent collagen, which loses fluorescence when degraded. (F) Addition of collagen to Mtb-infected cells reduces cell death, as analyzed by LDH release. (G) In a 3-D model where cells and Mtb are incorporated into an agar matrix with or without addition of collagen, incorporation of collagen with cells improves cellular survival after Mtb infection. Each experiment was performed a minimum of 2 times. Charts demonstrate the Mean + SEM of a representative experiment performed in triplicate. Scale bars: 100μm (A), 25μm (D, E).

Figure 5: A 3-dimensional bioelectrospray granuloma model demonstrates collagen improves cellular survival after Mtb-infection. Alginate microspheres were generated by bioelectrospraying a mixture of sterile alginate and PBMCs, with or without the incorporation of Mtb H37Rv and / or collagen into a gelling bath, which crosslinks alginate to form microspheres. (A) Microspheres imaged

immediately after bioelectrospraying by light microscopy. (B) Calcein staining of cells immediately after bioelectrospraying shows even distribution of cells throughout the microsphere. (C) Cells within microspheres phagocytose GFP-expressing Mtb after 4 days. GFP-expressing TB (green) is phagocytosed by monocytes (red) in the overlayed image (arrowheads indicate GFP-TB). (D) Large multicellular aggregates develop within Mtb-stimulated microspheres after 11 days, imaged after nuclear staining with DAPI. (E-F) IL-8 and MMP-1 progressively accumulate in media surrounding microspheres containing PBMCs cells infected with Mtb. (Broken line uninfected, filled line Mtb-infected). (G) Incorporation of collagen into microspheres improves survival of THP-1 cells after Mtb infection, analyzed by LDH release. (H) Similarly, PBMCs show greater survival when infected in microspheres containing collagen. (I) Collagen improves viability of PBMCs infected with Mtb within microspheres when analyzed by propidium iodide staining. (J) Total cell numbers are increased in Mtb-infected collagen-containing microspheres, analyzed by ATP released from viable cells. All experiments were performed a minimum of 2 times. For charts, data represent the mean +/- SEM of experiments performed in triplicate. Scale bars: 250μm (A, B), 10μm (C), 20μm (D).

Figure 6: A novel paradigm of TB pathology. (A) The current model of TB pathology proposes that cell death leads to caseous necrosis, which then causes lung extracellular matrix destruction, resulting in pulmonary cavitation and transmission. (B) Our data suggest that the initial pathological event is proteolytic destruction of the lung extracellular matrix, which then leads to cell death, resulting in the accumulation of caseous necrosis and cavitation.

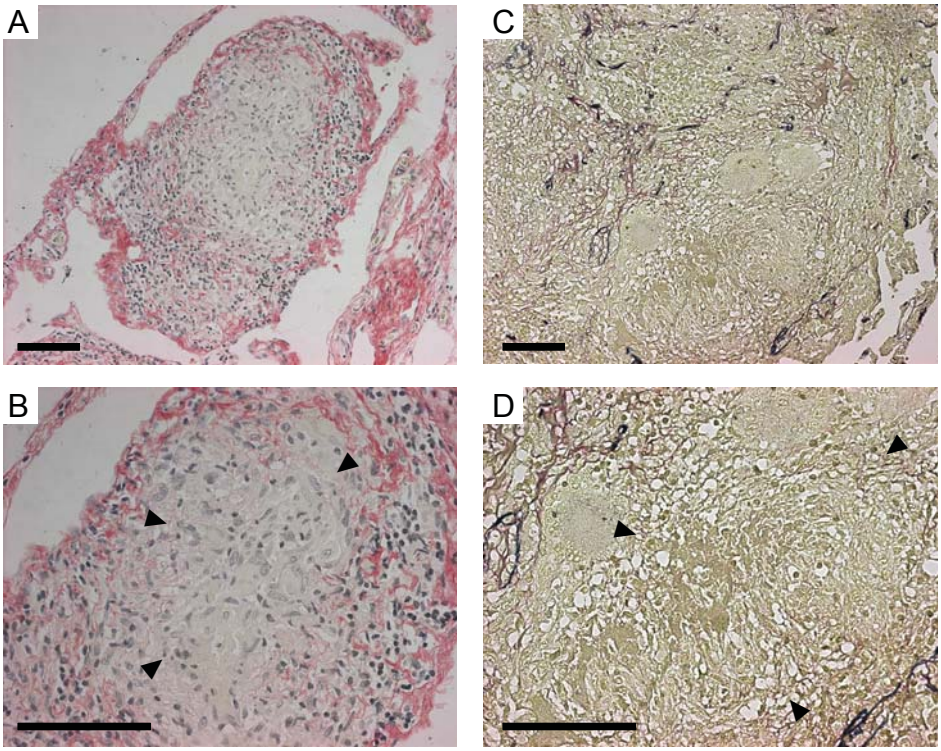

Figure 1

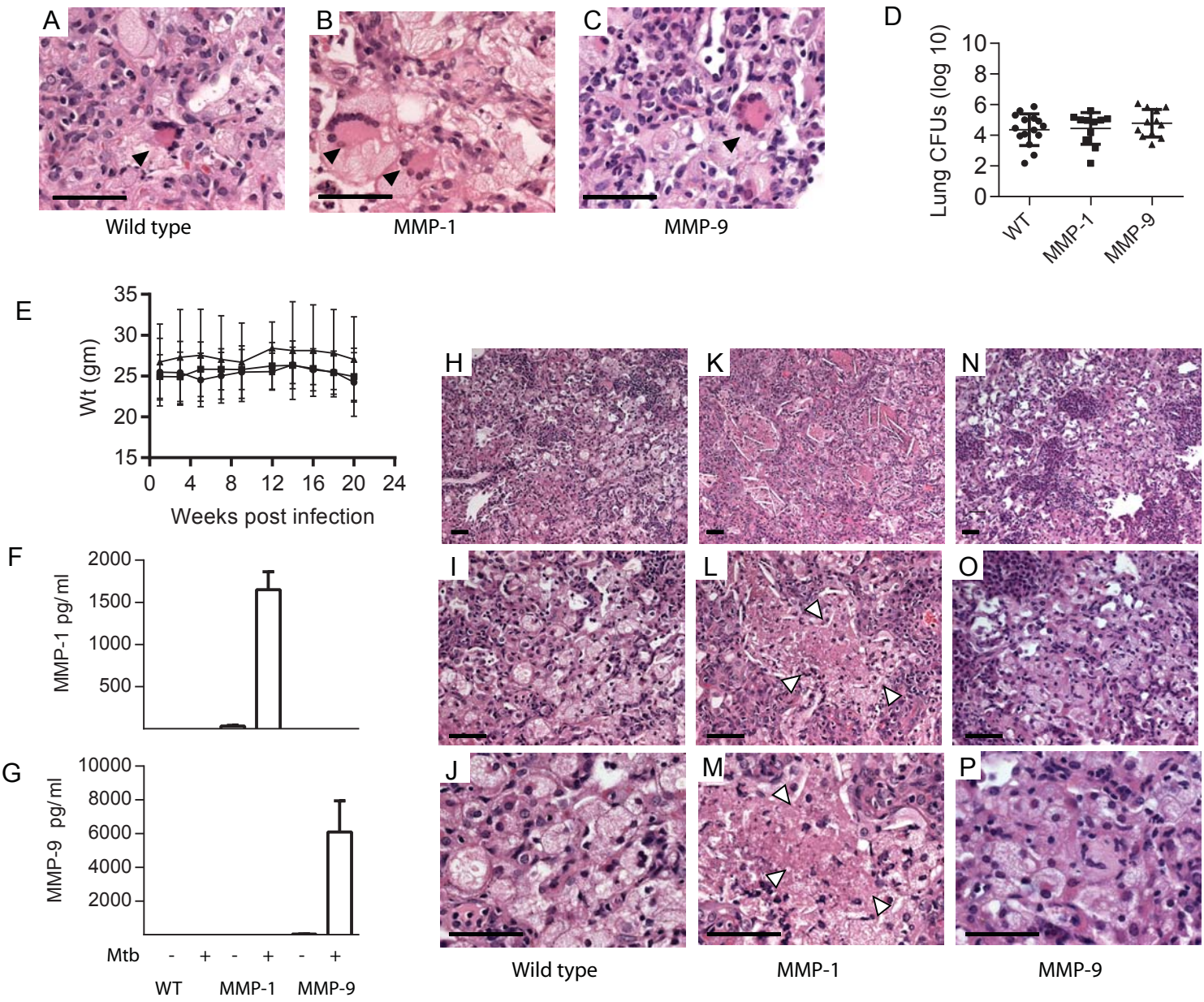
A
B
C
Wild type
MMP-1
MMP-9
D
Lung CFUs (log 10)
10
8
6
4
2
0
WT
MMP-1
MMP-9
E
Wt (gm)
35
30
25
20
15
0
4
8
12
16
20
24
Weeks post infection
F
MMP-1 pg/ml
2000
1500
1000
500
G
MMP-9 pg/ml
10000
8000
6000
4000
2000
Mtb
- + - + - +
WT
MMP-1
MMP-9
H
K
N
I
L
O
J
M
P
Wild type
MMP-1
MMP-9

Figure 2

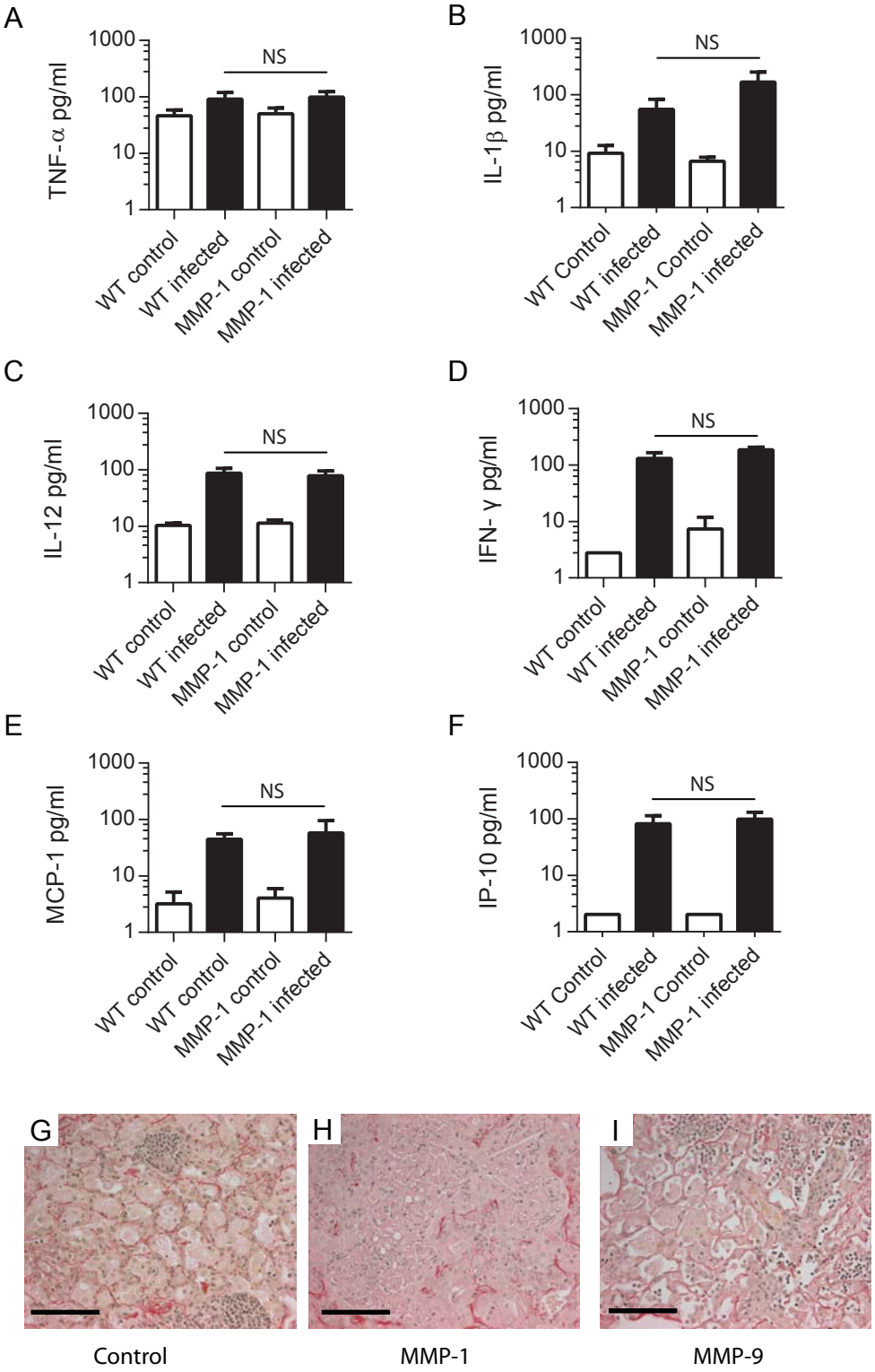
A
TNF-α pg/ml
1000
100
10
1
NS
WT control
WT infected
MMP-1 control
MMP-1 infected
B
IL-1β pg/ml
1000
100
10
1
NS
WT Control
WT infected
MMP-1 Control
MMP-1 infected
C
IL-12 pg/ml
1000
100
10
1
NS
WT control
WT infected
MMP-1 control
MMP-1 infected
D
IFN- γ pg/ml
1000
100
10
1
NS
WT control
WT infected
MMP-1 control
MMP-1 infected
E
MCP-1 pg/ml
1000
100
10
1
NS
WT control
WT control
MMP-1 control
MMP-1 infected
F
IP-10 pg/ml
1000
100
10
1
NS
WT Control
WT infected
MMP-1 Control
MMP-1 infected
G
H
I
Control
MMP-1
MMP-9

Figure 3

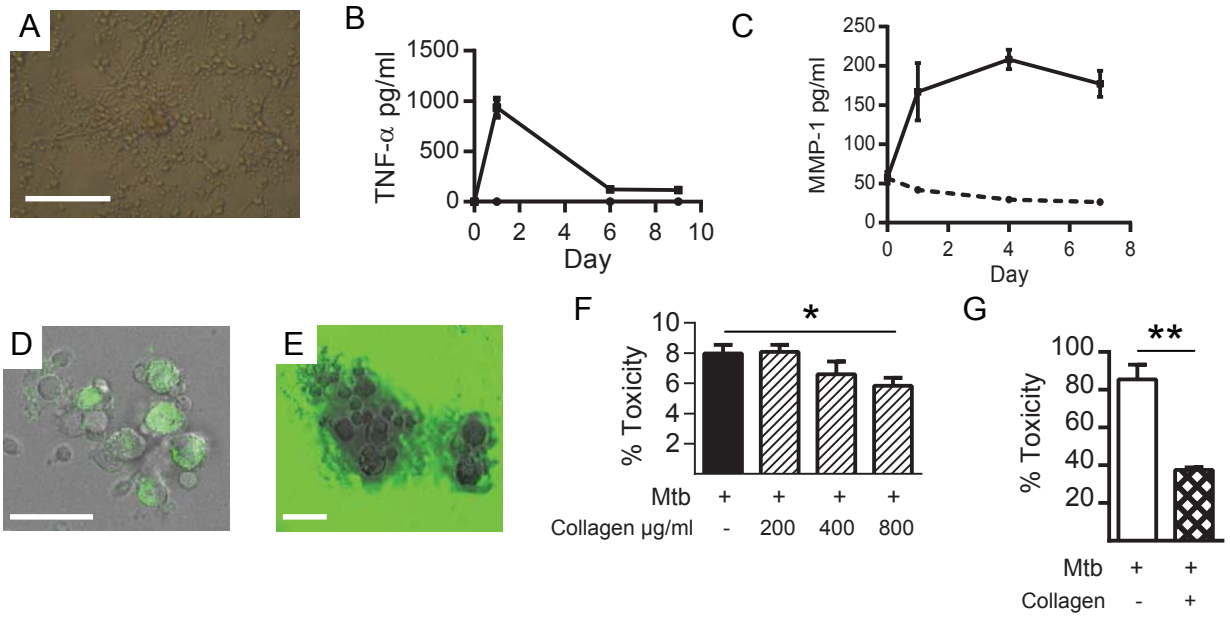
A
B
TNF-α pg/ml
1500
1000
500
0
0 2 4 6 8 10
Day
C
MMP-1 pg/ml
250
200
150
100
50
0
0 2 4 6 8
Day
D
E
F
% Toxicity
10
8
6
4
2
*
Mtb + + + +
Collagen µg/ml - 200 400 800
G
% Toxicity
100
80
60
40
20
**
Mtb + +
Collagen - +

Figure 4

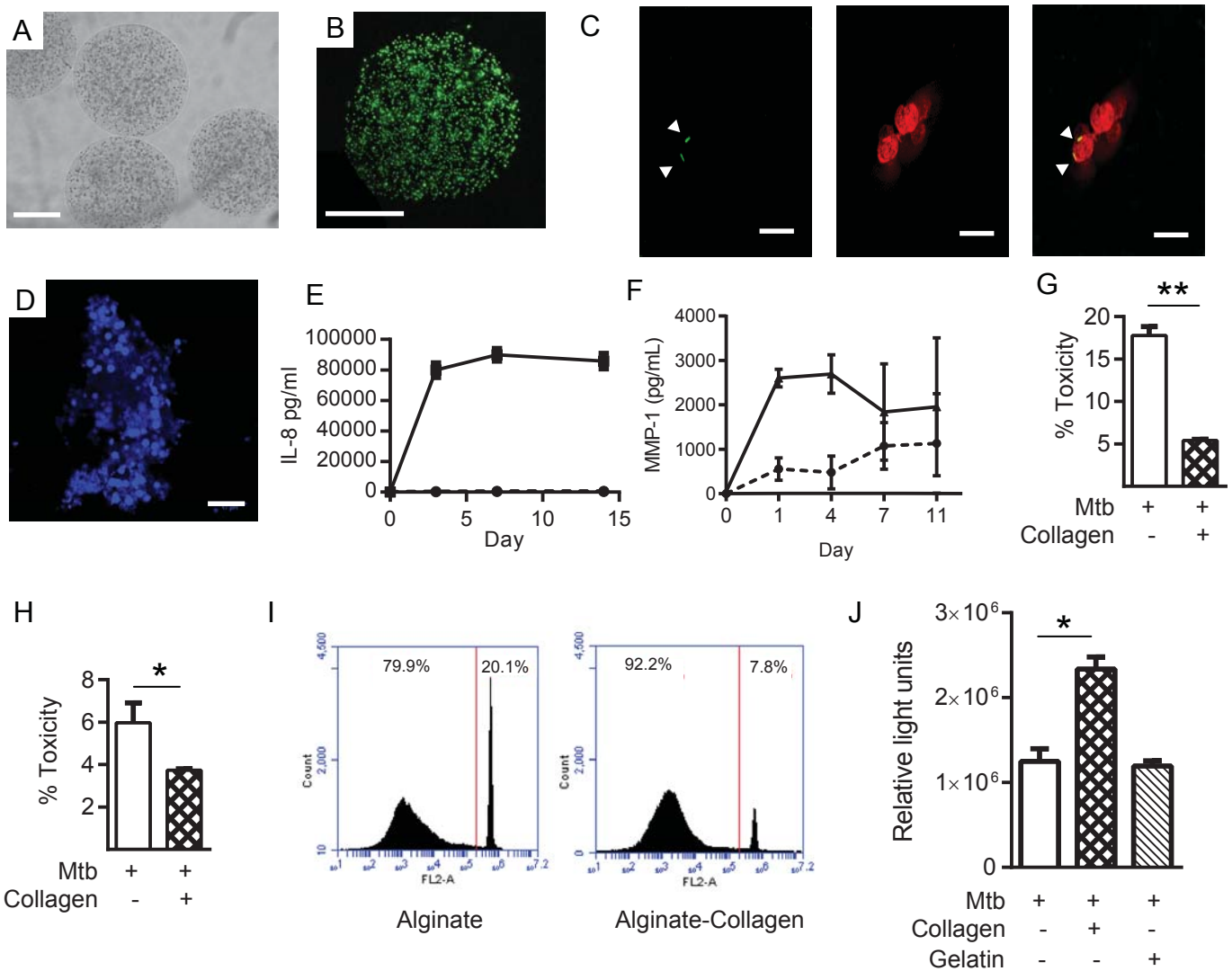
A
B
C
D
E
IL-8 pg/ml
100000
80000
60000
40000
20000
0
0
5
10
15
Day
F
MMP-1 (pg/mL)
4000
3000
2000
1000
0
0
1
4
7
11
Day
G
**
% Toxicity
20
15
10
5
Mtb + +
Collagen - +
H
*
% Toxicity
8
6
4
2
Mtb + +
Collagen - +
I
79.9%
20.1%
92.2%
7.8%
Count
FL2-A
Alginate
Alginate-Collagen
J
*
Relative light units
3×10^6
2×10^6
1×10^6
0
Mtb + + +
Collagen - + -
Gelatin - - +

Figure 5

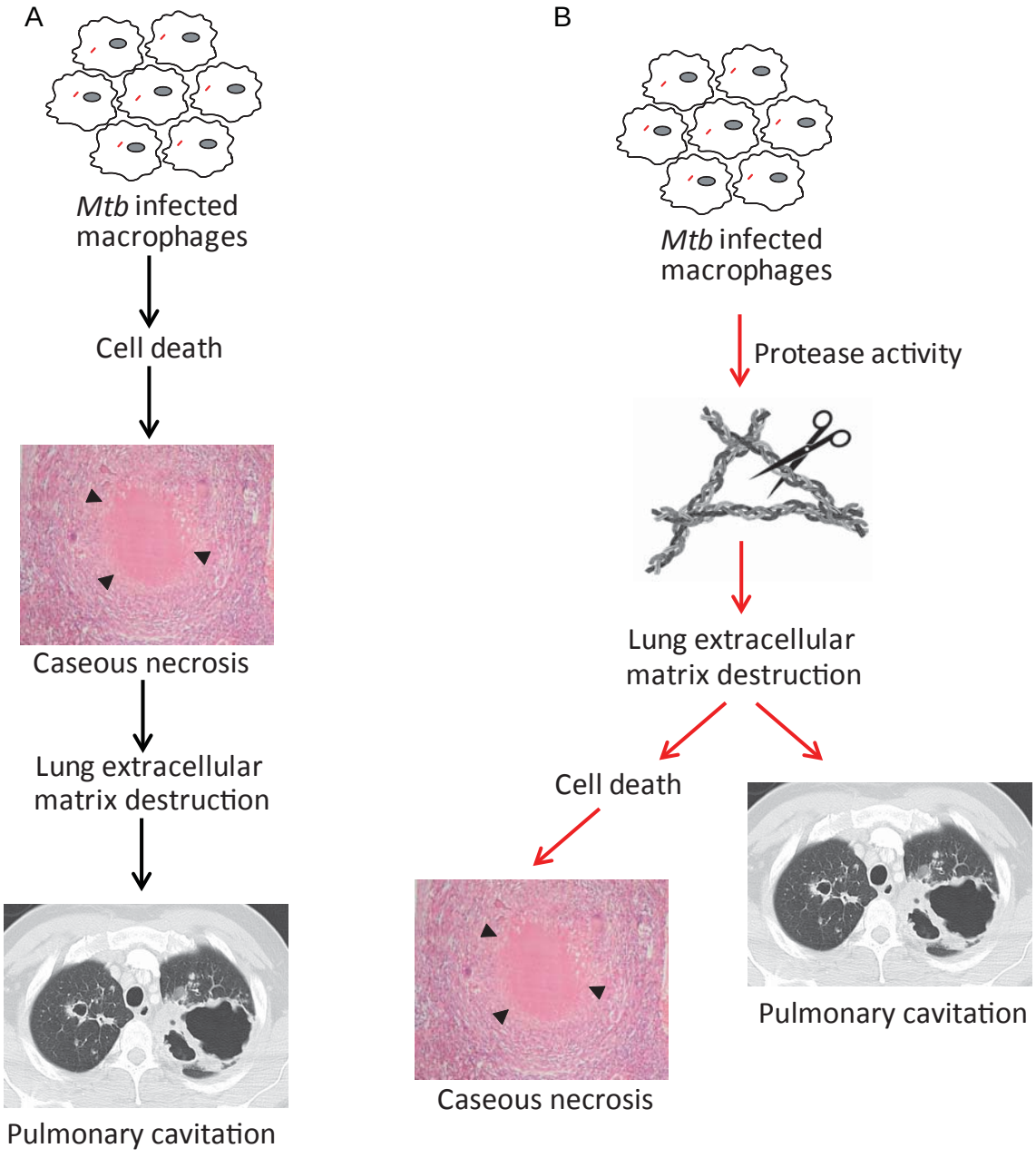
A
Mtb infected macrophages
Cell death
Caseous necrosis
Lung extracellular matrix destruction
Pulmonary cavitation
B
Mtb infected macrophages
Protease activity
Lung extracellular matrix destruction
Cell death
Caseous necrosis
Pulmonary cavitation

Figure 6

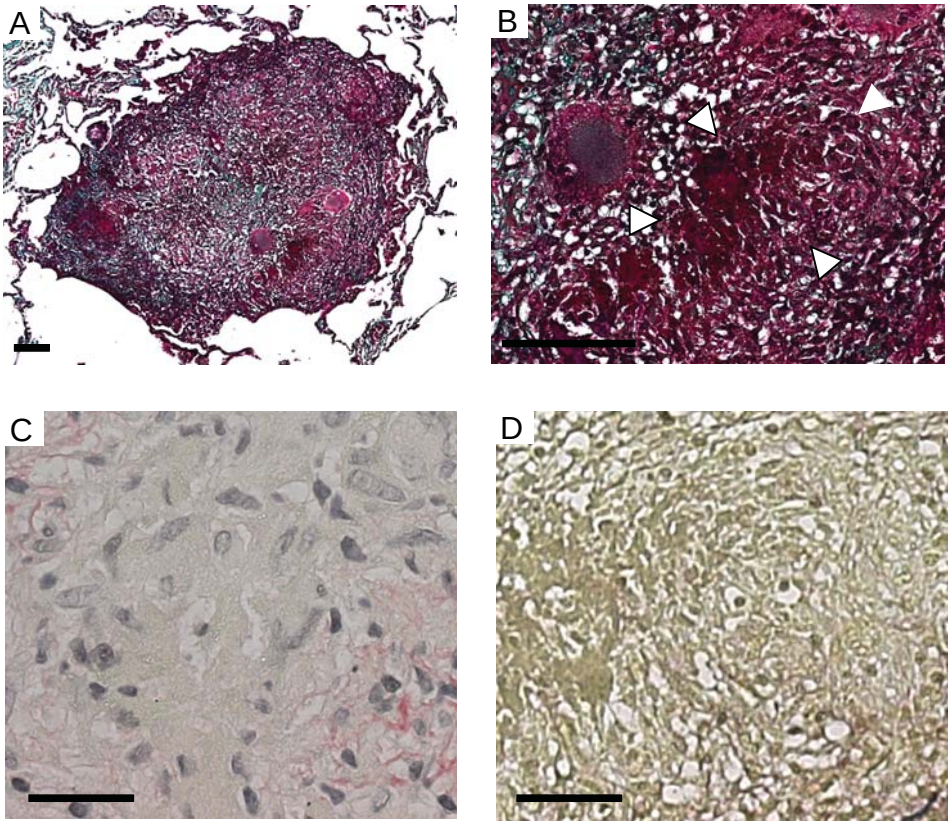

Figure S1: A, B. Lung biopsies from patients under investigation for lung carcinoma but with a final diagnosis of TB were stained by Masson's trichrome. All extracellular matrix stains blue-green. Extracellular matrix is absent in all regions of caseous necrosis, which stains deep purple (highlighted by white arrowheads). Images are representative of 5 TB patient lung biopsies that were studied. Scale bars 100μm. **C, D.** High magnification images from Figure 1 to demonstrate the areas of necrosis at high power. Collagen (C) and elastin (D) are absent within areas of necrosis. Scale bars 25μm.

Wild type

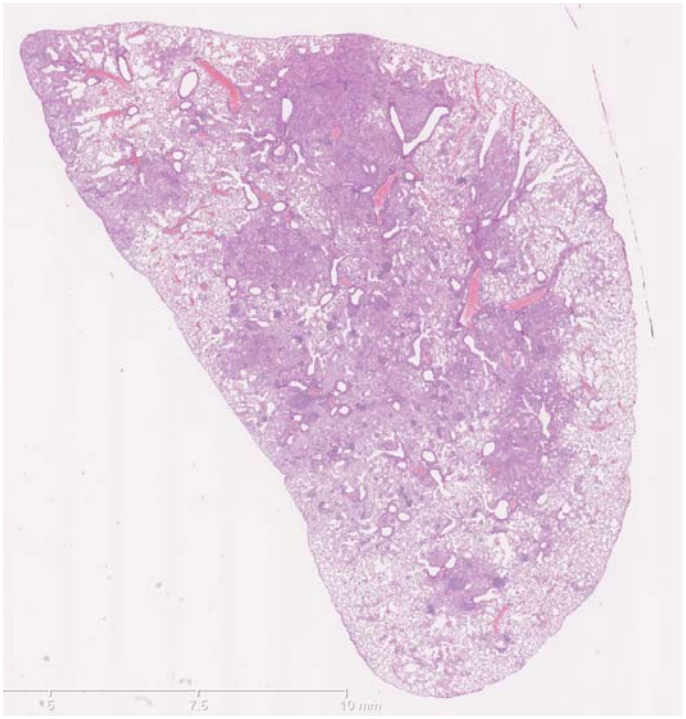

MMP-1

MMP-9

Figure S2: Images of the whole lung sections of mice that the higher power magnifications are presented in Figure 2H-P. The entire lung sections are presented from which the high power magnifications are taken to demonstrate that total lung inflammation does not differ between the 3 mouse strains.

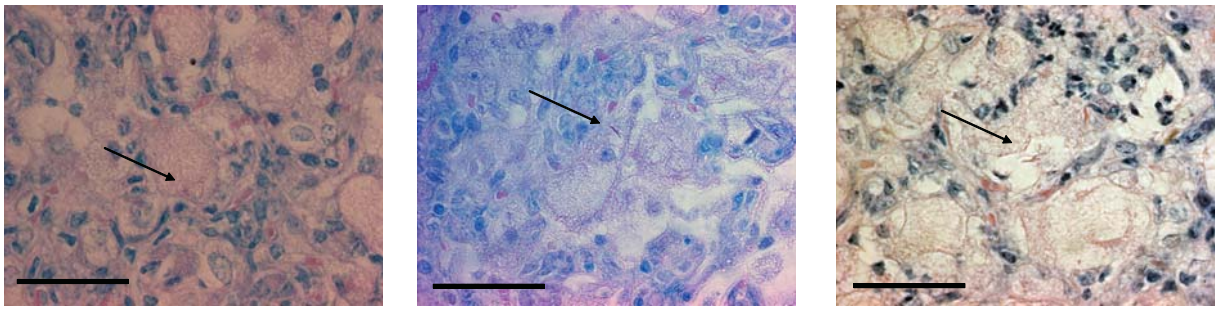

Figure S3: Acid fast bacilli (arrows) are present in areas of foamy macrophage infiltration in lungs of infected mice on Ziehl-Neelsen staining. Data are representative of at minimum of 5 mice per group. Original magnification x100, scale bar 20 μm.

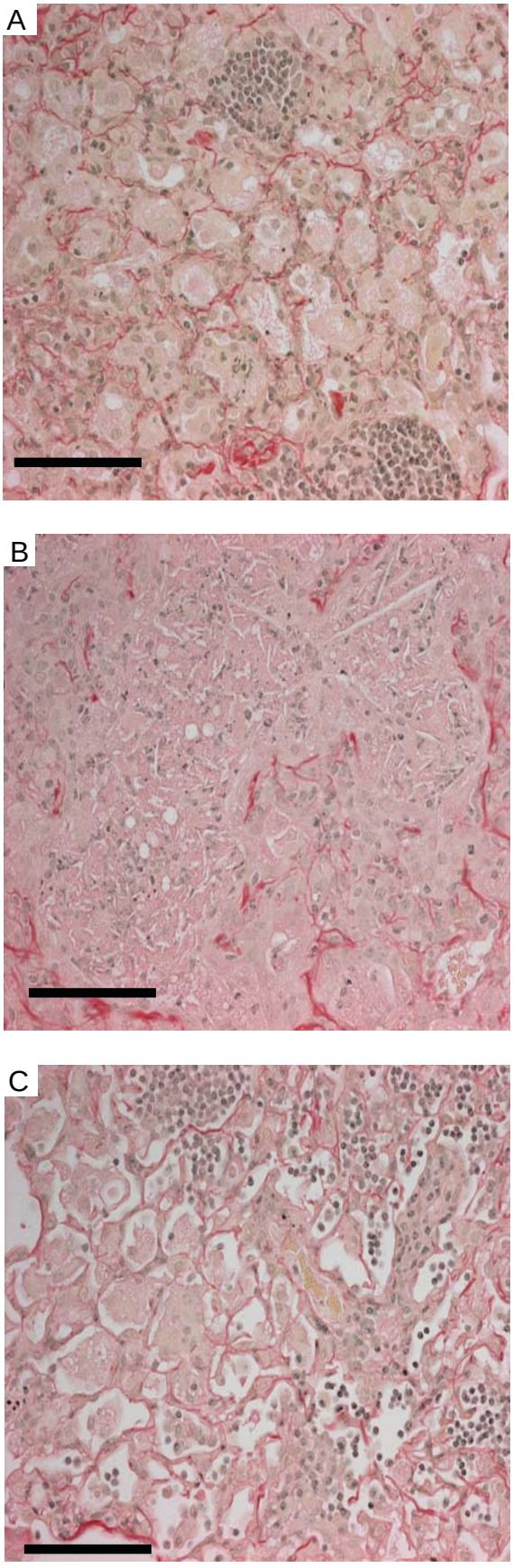

Figure S4: Enlarged images of Figure 3, panels G, H and I to demonstrate the microscopic differences. Collagen is absent in areas of caseous necrosis, whereas collagen is present where cells maintain normal morphology. A, wild type, B MMP-1, C MMP-9-expressing mice.

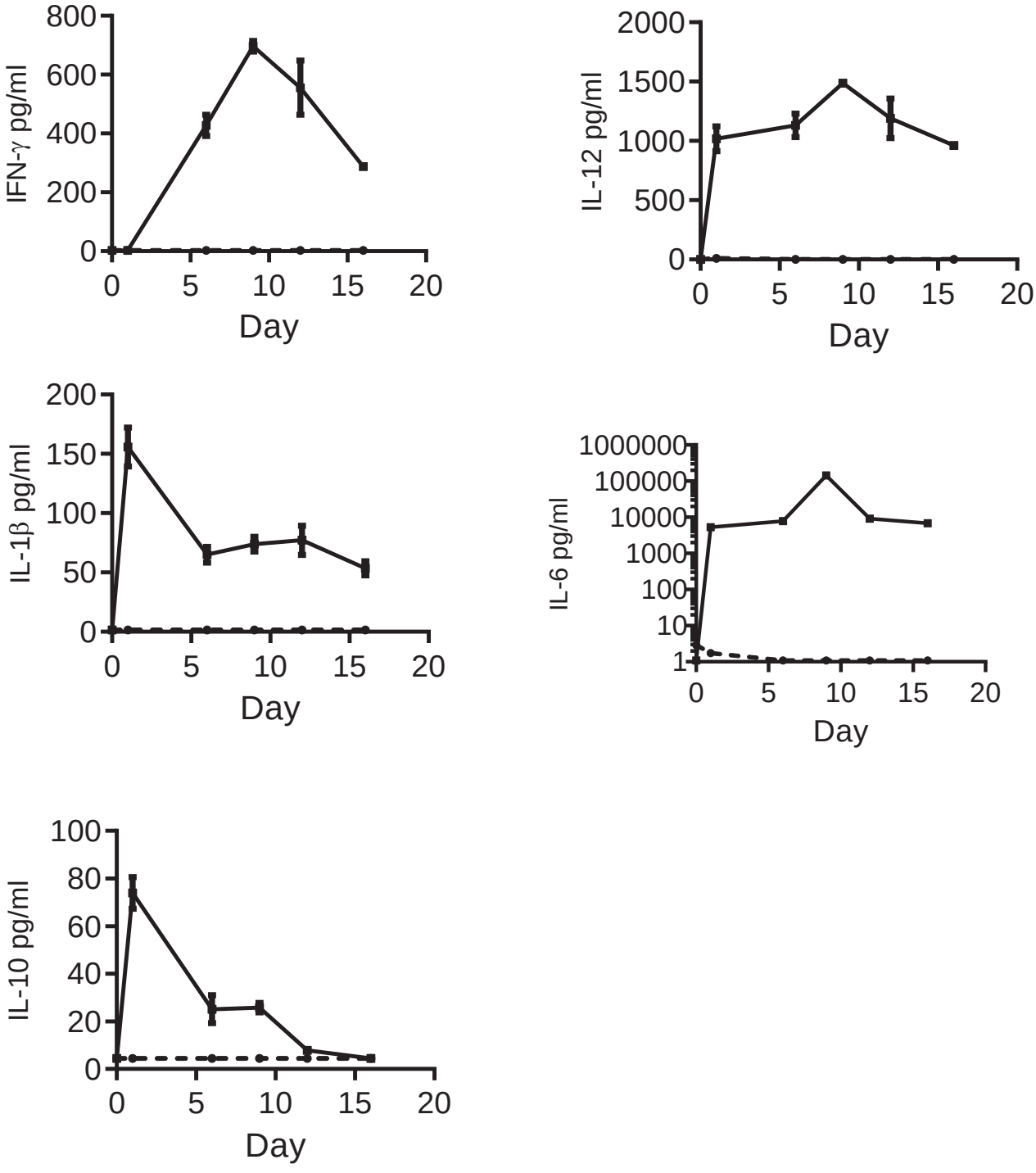

Figure S5: Cytokines progressively accumulate in cell culture supernatant of Mtb-infected PBMCs. Broken line, uninfected PBMCs, filled line Mtb-infected PBMCs. Data are mean + SD of an experiment performed in triplicate, and represent an experiment performed on 2 occasions in triplicate.